

**Showcasing research from Professor Dillip K. Chand and group - IoE Center of Molecular Architecture, IIT Madras, India.**

A pair of conjoined trinuclear sub-frameworks in a pentanuclear double-cavity discrete coordination cage

In line with our “Tryst with MCDCC” (Multi-cavity Discrete Coordination Cages), we reveal here an architectural adventure undertaken at molecular level *via* integrative self-sorting of Pd(II) and designer organic ligands. Ever since we introduced a pair of conjoined dinuclear sub-frameworks in the form of a Pd<sub>3</sub>L<sub>4</sub> type trinuclear double-cavity Pd(II)-based cage, we had a dream of conjoining a pair of trinuclear sub-frameworks too. A decade past the Pd<sub>3</sub>L<sub>4</sub>, enters the awaited Pd<sub>5</sub>L<sub>4</sub>L'<sub>4</sub> type pentanuclear double-cavity Pd(II)-based cage; also, the lower symmetry version of the mixed ligated cage.

Two Lotus Flowers by Pixabay, Lunar eclipse by Julia Barthold, both *via* Pexels.com.

**As featured in:**





See Dillip Kumar Chand *et al.*,  
*Chem. Sci.*, 2024, **15**, 11287.

Cite this: *Chem. Sci.*, 2024, 15, 11287

All publication charges for this article have been paid for by the Royal Society of Chemistry

# A pair of conjoined trinuclear sub-frameworks in a pentanuclear double-cavity discrete coordination cage†

 Shruti Sharma, Shobhana Krishnaswamy,  Soumyakanta Prusty‡ and Dillip Kumar Chand \*

Combination of Pd(II) with selected bis-monodentate ligands produces the familiar multinuclear Pd<sub>m</sub>L<sub>2m</sub> type self-assembled “single-cavity discrete coordination cages” (SCDCC). If the ligand provides parallel coordination vectors, then it forms a binuclear Pd<sub>2</sub>L<sub>4</sub> type cage, whereas utilization of ligands having appropriately divergent coordination vectors results in specific higher nuclear complexes. In contrast, preparation of emergent “multi-cavity discrete coordination cages” (MCDCC) using Pd(II) and designer ligands is quite captivating where the neighboring cavities of the framework are conjoined with each other through a common metal center. A pair of conjoined binuclear Pd<sub>2</sub>L<sub>4</sub> type sub-frameworks are present in a trinuclear Pd<sub>3</sub>L<sub>4</sub> type double-cavity cage prepared from Pd(II) and a tris-monodentate ligand having parallel coordination vectors. The present work envisioned a design to make double-cavity coordination cages having a pair of conjoined trinuclear Pd<sub>3</sub>L<sub>6</sub> type sub-frameworks. To fulfill the objective we combined Pd(II) with a mixture of designer bis-monodentate ligand (L) and tris-monodentate ligand (L') in a 5 : 4 : 4 ratio in one pot to afford the targeted pentanuclear Pd<sub>5</sub>L<sub>4</sub>L'<sub>4</sub> type cage. The choice of bis-monodentate ligand L is based on the divergent nature of the coordination vectors suitable to produce a Pd<sub>3</sub>L<sub>6</sub> type SCDCC. The tris-monodentate ligand L' having two arms is designed in such a manner that each of the arms reasonably resembles L. Study of the complexation behavior of Pd(II) with L' provided additional guiding factors essential for the successful making of Pd<sub>5</sub>L<sub>4</sub>L'<sub>4</sub> type MCDCC by integrative self-sorting. A few other MCDCC including lower symmetry versions were also prepared in the course of the work.

Received 15th February 2024

Accepted 11th June 2024

DOI: 10.1039/d4sc01078g

rsc.li/chemical-science

## 1 Introduction

Building of coordination architectures by a metal-driven self-assembly route using the participants from a library of metal and ligand components has strategic importance in supramolecular chemistry.<sup>1–9</sup> Combination of Pd(II) with one type of symmetrical bis-monodentate ligand to prepare “single-cavity discrete coordination cages” (SCDCC) of Pd<sub>m</sub>L<sub>2m</sub> formulations is well known.<sup>10–15</sup> Fig. 1A and B depict binuclear Pd<sub>2</sub>L<sub>4</sub> and trinuclear Pd<sub>3</sub>L<sub>6</sub> type cages (simplest but most studied Pd<sub>m</sub>L<sub>2m</sub>). Diverging coordination vectors and appropriate bend angles of the ligands are important parameters that decide the nuclearity of the ensuing cages. Preparation of Pd(II)-based low-symmetry SCDCC has been achieved by either mixing of Pd(II) with a designer unsymmetrical ligand<sup>14,16–21</sup> to afford orientational

selectivity of ligand components, or mixing of Pd(II) with more than one type of ligand<sup>14,22–26</sup> targeting mixed ligated integrative self-sorting.

Making the rare “multi-cavity discrete coordination cages” (MCDCC) is quite captivating because multiple but defined number of cavities are present in their architectures.<sup>14,27–29</sup> This is in contrast to the single-cavity and infinite cavities of the prevalent SCDCC and “metal organic frameworks” (MOF), respectively.<sup>30–33</sup> We introduced<sup>34</sup> a double-cavity trinuclear Pd<sub>3</sub>L<sub>4</sub> type MCDCC (Fig. 1C(i)); such conjoined cages of Pd<sub>3</sub>L<sub>4</sub> type have received considerable attention<sup>14,35–39</sup> recently. In the framework of a Pd<sub>3</sub>L<sub>4</sub> type cage there are two units of Pd<sub>2</sub>L<sub>4</sub> type sub-framework that are apparently conjoined with each other using a common square planar coordination environment of a Pd(II) centre. Low-symmetry Pd<sub>3</sub>L<sub>4</sub> cages possessing two unequal sized Pd<sub>2</sub>L<sub>4</sub> sub-frameworks have been reported<sup>40–42</sup> as shown in Fig. 1D(i). Another class of double-cavity tetranuclear conjoined cage where a Pd<sub>2</sub>L<sub>4</sub> type sub-framework is conjoined with a Pd<sub>3</sub>L<sub>6</sub> type sub-framework (see Fig. 1E) has been reported<sup>40</sup> by us that is a sole example of its own type.

In the present work we have successfully lowered the symmetry of the above mentioned tetranuclear MCDCC (compare Fig. 1E with G). However, the major disclosure of this

IoE Center of Molecular Architecture, Department of Chemistry, Indian Institute of Technology Madras, Chennai 600036, India. E-mail: dillip@iitm.ac.in

† Electronic supplementary information (ESI) available. CCDC 2326106, 2326107 and 2326108. For ESI and crystallographic data in CIF or other electronic format see DOI: <https://doi.org/10.1039/d4sc01078g>

‡ Current address: Department of Chemistry, VIT-AP University, Amaravati 522237, India.



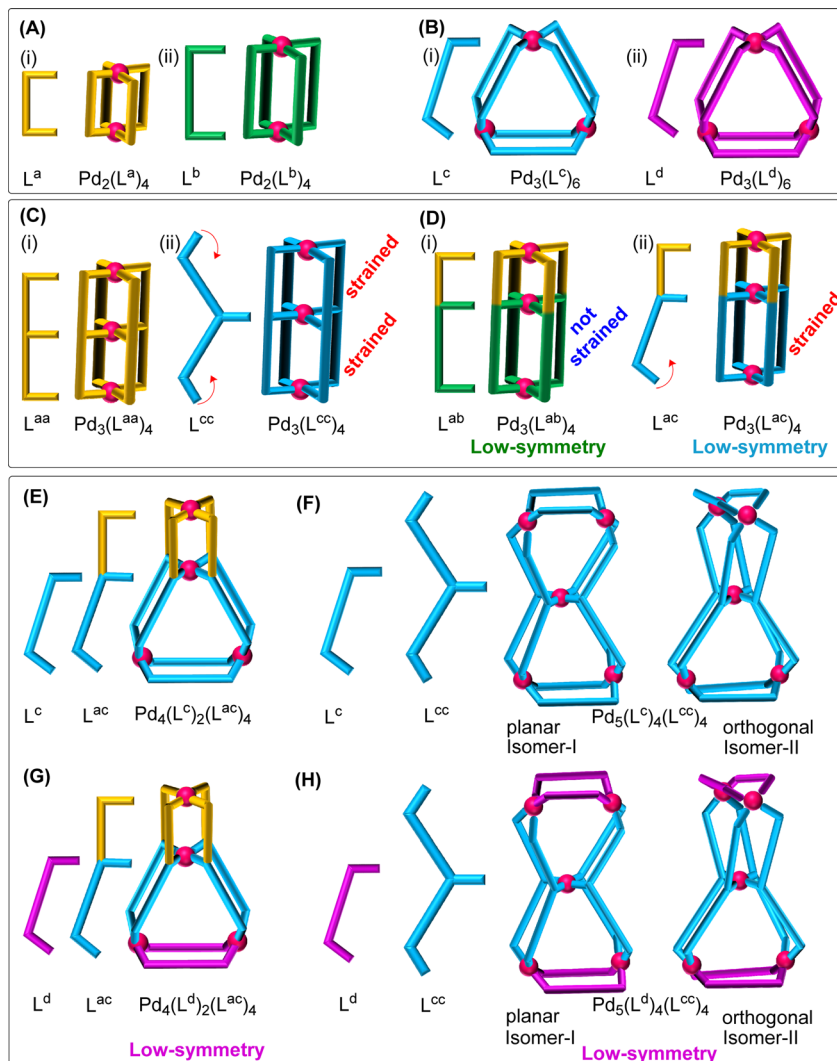


Fig. 1 Cartoon representation depicting Pd(II)-based (A) and (B) single-cavity bi-/trinuclear regular cages, and (C)–(H) double-cavity tri-/tetra-/pentanuclear conjoined cages (the constituent ligands are also shown). The depicted conjoined cages have characteristic metal sharing where apparent conjoining of (C) a “binuclear” with a “binuclear” of equal size, (D) a “binuclear” with a “binuclear” of unequal size, (E)/(G) a “binuclear” with a “trinuclear”, and (F)/(H) a “trinuclear” with a “trinuclear” are presented.

work is the achievement of an entirely new design that is a double-cavity pentanuclear conjoined cage where a triangular  $\text{Pd}_3\text{L}_6$  type sub-framework is conjoined with another  $\text{Pd}_3\text{L}_6$  type sub-framework as shown in Fig. 1F; further, the symmetry of the pentanuclear cage could be lowered as shown in Fig. 1H. One-pot complexation of Pd(II) with a bis-monodentate ligand and a tris-monodentate ligand in a 5 : 4 : 4 ratio is required for achieving the targeted pentanuclear complexes. A thorough analysis of the results obtained provides us with necessary guidelines for the making of double-cavity pentanuclear MCDCC.

## 2 Results and discussion

### Design of the double-cavity pentanuclear conjoined cage

Making of the double-triangle type pentanuclear conjoined cages, depicted in Fig. 1F and H, *via* complexation of Pd(II) with tailored ligands is the primary objective of this work. Designing

aspects of ligands to achieve the targeted cages is described hereafter. Complexation of Pd(II) with a bis-monodentate ligand such as  $\text{L}^c$  (or  $\text{L}^d$ ) having appropriate divergence of the coordination vector, hence suitable bend angle, would form the well-known  $\text{Pd}_3\text{L}_6$  type trinuclear framework, *i.e.*  $[\text{Pd}_3(\text{L}^c)_6]^{6+}$  (or  $[\text{Pd}_3(\text{L}^d)_6]^{6+}$ ), shown in Fig. 1B.<sup>43</sup> It should be possible to prepare tris-monodentate ligands such as  $\text{L}^{\text{cc}}$  and  $\text{L}^{\text{dd}}$  by taking inspiration from  $\text{L}^c$  and  $\text{L}^d$  type ligands (see Fig. 1C(ii) for  $\text{L}^{\text{cc}}$ ). Combination of Pd(II) with  $\text{L}^{\text{cc}}$  would not result in a discrete structure keeping the  $\text{Pd}_3\text{L}_6$  type sub-framework intact. Thus, it might form a strained coordination cage like  $[\text{Pd}_3(\text{L}^{\text{cc}})_4]^{6+}$  (Fig. 1C(ii)) and/or oligomerized complexes unless the ligand finds way to form an alternate but sufficiently stable cage framework; the same comments apply for complexation of Pd(II) with  $\text{L}^{\text{dd}}$ .

We asked ourselves whether or not a one-pot mixture of Pd(II),  $\text{L}^c$  and  $\text{L}^{\text{cc}}$  would result in integrative self-sorting. The



answer being: in order to avoid the imposition of strain/oligomerization mentioned above, narcissistic (or statistical) self-sorting would not occur, hence giving way to integrative self-sorting from a mixture of Pd(II), L<sup>c</sup> and L<sup>cc</sup> in a 5 : 4 : 4 ratio to afford a double-cavity conjoined cage like [Pd<sub>5</sub>(L<sup>c</sup>)<sub>4</sub>(L<sup>cc</sup>)<sub>4</sub>]<sup>10+</sup> (Fig. 1F). Symmetry of this pentanuclear complex can be lowered locally at the trinuclear moieties by mixing Pd(II), L<sup>d</sup> and L<sup>cc</sup> to prepare a conjoined cage, *i.e.* [Pd<sub>5</sub>(L<sup>d</sup>)<sub>4</sub>(L<sup>cc</sup>)<sub>4</sub>]<sup>10+</sup> (Fig. 1H), on the condition that the ligands L<sup>c</sup> and L<sup>d</sup> are of comparable lengths or averaged non-bonded distances between Pd(II) centres in [Pd<sub>3</sub>(L<sup>c</sup>)<sub>6</sub>]<sup>6+</sup> are comparable with that of [Pd<sub>3</sub>(L<sup>d</sup>)<sub>6</sub>]<sup>6+</sup>. Similarly, cages like [Pd<sub>5</sub>(L<sup>d</sup>)<sub>4</sub>(L<sup>dd</sup>)<sub>4</sub>]<sup>10+</sup> and [Pd<sub>5</sub>(L<sup>c</sup>)<sub>4</sub>(L<sup>dd</sup>)<sub>4</sub>]<sup>10+</sup> are conceivable. However, the process of integrative self-sorting might get inhibited and hence narcissistic/statistical self-sorting might partially or completely take over if the ligand L<sup>cc</sup> or L<sup>dd</sup> finds alternate stable architectures without involving the ancillary ligand L<sup>c</sup> or L<sup>d</sup>.

The designs shown in Fig. 1F and H are practically realised in the present work with logical ligand designs where the orthogonal isomer-II is formed in preference to the planar isomer-I. Detailed investigation of the ligand systems of this work assisted in the mapping of Pd(II)-coordination behaviour of individual ligands (L<sup>cc</sup> and L<sup>dd</sup>) with the prospect of their participation in narcissistic or integrative self-sorting in the presence of an ancillary ligand like L<sup>c</sup> or L<sup>d</sup>. In the course of our research work, all cage varieties shown in Fig. 1 (except 1A, 1C(i) and 1D(i)) were prepared.

### Synthesis of ligands L1 to L6

For a systematic study, we have prepared a series of pyridine-appended semi-flexible/-rigid organic ligands (L1–L6) as shown in Fig. 2. This series includes symmetrical bis-monodentate ligands (L1 and L2), unsymmetrical tris-monodentate ligands (L3 and L4), and symmetrical tris-monodentate ligands (L5 and L6). The conformations of

ligands shown in Fig. 2 are selected on the basis of their probable conformation in the targeted complexes (as learned during the course of the work); some of the related conformers of L1, L2, L5 and L6 are shown in ESI Fig. S1 and S2.†

The ligands L1 and L2 were synthesized, by slight modification of known procedures,<sup>44,45</sup> in one-step condensation reactions of two equivalents of nicotinic acid with one equivalent of 1,4-dihydroxybenzene and 1,5-dihydroxynaphthalene, respectively (ESI Schemes S1 and S2†). Synthesis of the ligands L3–L6 required esterification reactions using four possible combinations comprising of one of the mono-/dicarboxylic acid precursors (from (i) pyridine-3,5-dicarboxylic acid and (ii) 5-((pyridin-3-ylmethoxy)carbonyl)nicotinic acid, A) and one of the monohydroxy precursors (from (i) 4-hydroxyphenyl nicotinate, B, and (ii) 5-hydroxynaphthalene-1-yl nicotinate, C). The precursor A was prepared following a method established in our laboratory<sup>40</sup> whereas B and C were prepared by condensation of nicotinic acid with three equivalents of 1,4-dihydroxybenzene and 1,5-dihydroxynaphthalene, respectively (ESI Schemes S3 and S4†). Then, the ligands L3 and L4 were synthesized in one-step condensation reactions of the monocarboxylic acid A with monohydroxy compounds B and C, respectively (ESI Schemes S5 and S6†). The ligands L5 and L6 were obtained in one-step condensation reactions of pyridine-3,5-dicarboxylic acid with B and C, respectively (ESI Schemes S7 and S8†). All the ligands except L5 are soluble in DMSO/DMSO-*d*<sub>6</sub>; ligand L5 is sparingly soluble in CHCl<sub>3</sub>/CDCl<sub>3</sub>. The precursors B and C and all the ligands were characterized by ESI-MS and various NMR techniques including <sup>1</sup>H, <sup>13</sup>C (not for L5), H–H COSY, C–H COSY (not for L5) and H–H NOESY (not for L1 and L2) (ESI Fig. S3–S46†). The ligands L1 and L2 are known<sup>44,45</sup> whereas the ligands L3–L6 are new. However, L1 has not been used for complexation with any metal ions but it is ribosylated at pyridine nitrogen positions to prepare compounds of pharmaceutical values.<sup>44</sup> The ligand L2 binds as a guest in the cleft of a specific bis-zinc porphyrin host.<sup>45</sup>

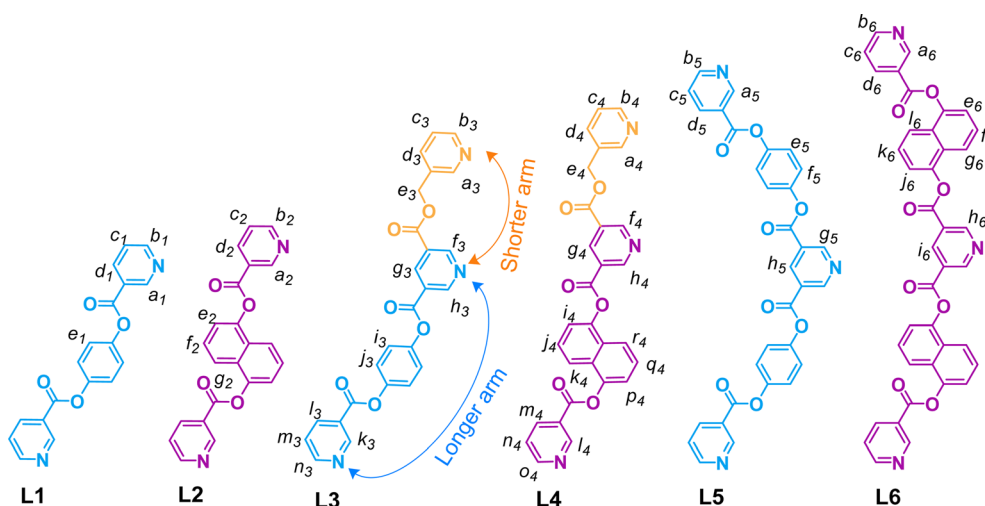


Fig. 2 Chemical structures of the symmetrical bis-monodentate (L1, L2), unsymmetrical tris-monodentate (L3, L4) and symmetrical tris-monodentate (L5, L6) ligands.

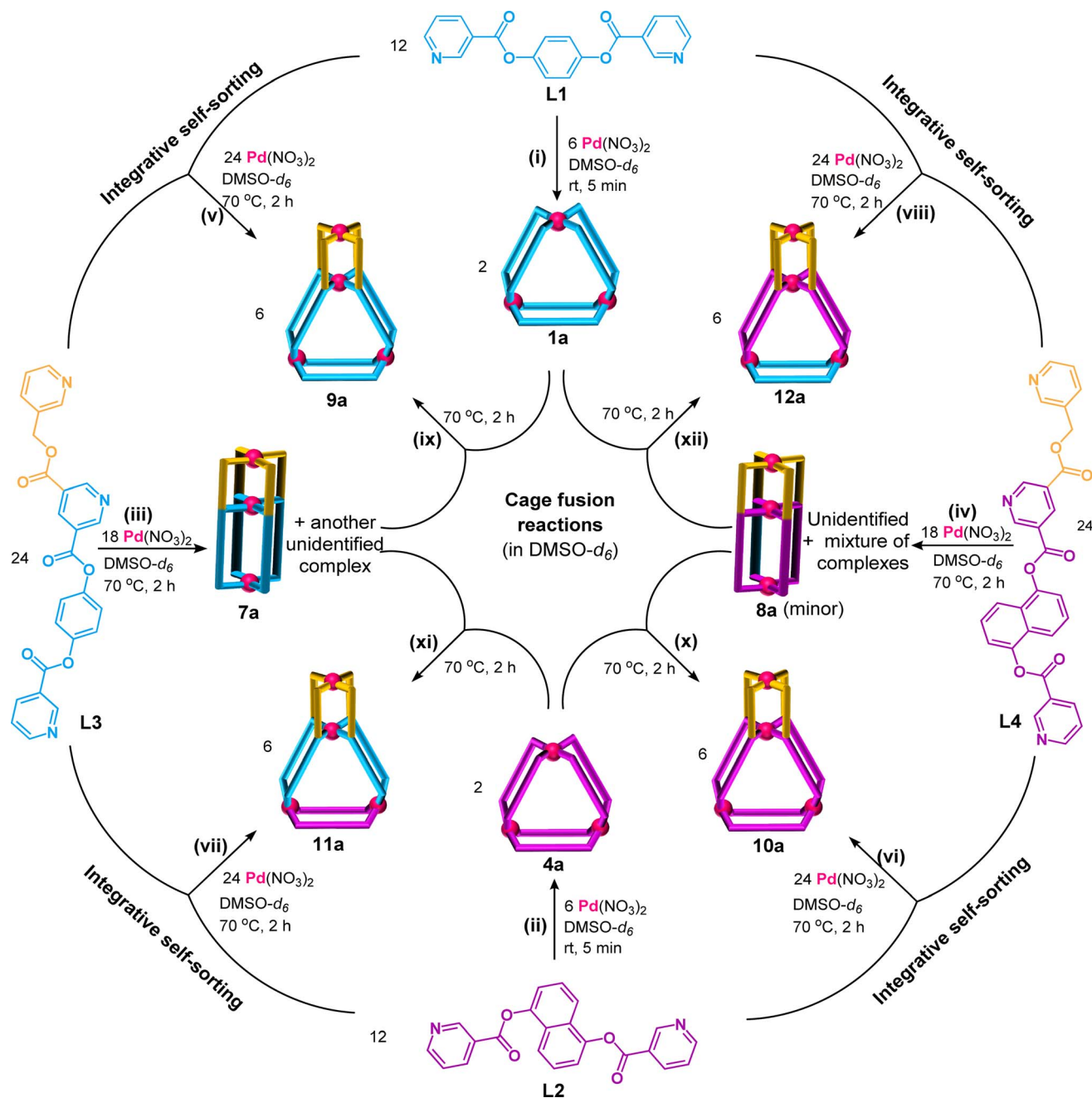


### Complexation of Pd(II) separately with bis-monodentate ligands L1 and L2

Complexation of Pd(NO<sub>3</sub>)<sub>2</sub> with the ligand L1 in a 1 : 2 ratio (Scheme 1(i), ESI Scheme S9<sup>†</sup>) was performed in DMSO-*d*<sub>6</sub> at room temperature (27 °C) keeping 10 mM as the concentration with respect to Pd(II). Spontaneous formation (within 5 min) of a single discrete product was confirmed by monitoring the reaction mixture using <sup>1</sup>H NMR spectroscopy. The spectrum (Fig. 3(ii)) showed a single set of downfield-shifted sharp signals

with substantial shift for inward- and outward-pointing α-pyridine protons (Δδ = 0.85 and 0.87 ppm for H<sub>a1</sub> and H<sub>b1</sub>, respectively) with respect to the free ligand (Fig. 3(i and ii)). ESI-MS study indicated the formation of a Pd<sub>3</sub>L<sub>6</sub> type complex: [Pd<sub>3</sub>(L1)<sub>6</sub>](NO<sub>3</sub>)<sub>6</sub>, **1a** (ESI Fig. S54<sup>†</sup>).

It is reported that complexation of Pd(II) with L1' (a positional isomer of L1) containing a *meta*-phenylene spacer also formed a Pd<sub>3</sub>L<sub>6</sub> type complex: [Pd<sub>3</sub>(L1')<sub>6</sub>](NO<sub>3</sub>)<sub>6</sub>, **1a'**. However, the complexation reaction at lower and higher concentrations



Scheme 1 ((i) to (iv)) Complexation of Pd(NO<sub>3</sub>)<sub>2</sub> with one type of ligand, ((v) to (viii)) complexation of Pd(NO<sub>3</sub>)<sub>2</sub> with two types of ligands, and ((ix) to (xii)) cage fusion reactions, to prepare (i) [Pd<sub>3</sub>(L1)<sub>6</sub>](NO<sub>3</sub>)<sub>6</sub>, **1a**; (ii) [Pd<sub>3</sub>(L2)<sub>6</sub>](NO<sub>3</sub>)<sub>6</sub>, **4a**; (iii) [Pd<sub>4</sub>(L3)<sub>4</sub>](NO<sub>3</sub>)<sub>8</sub>, **7a**; (iv) [Pd<sub>4</sub>(L4)<sub>4</sub>](NO<sub>3</sub>)<sub>8</sub>, **8a** and unidentified complexes; (v)/(ix) [Pd<sub>4</sub>(L1)<sub>2</sub>(L3)<sub>4</sub>](NO<sub>3</sub>)<sub>10</sub>, **9a**; (vi)/(x) [Pd<sub>4</sub>(L2)<sub>2</sub>(L4)<sub>4</sub>](NO<sub>3</sub>)<sub>10</sub>, **10a**; (vii)/(xi) [Pd<sub>4</sub>(L1)<sub>2</sub>(L3)<sub>4</sub>](NO<sub>3</sub>)<sub>10</sub>, **11a**; and (viii)/(xii) [Pd<sub>4</sub>(L1)<sub>2</sub>(L4)<sub>4</sub>](NO<sub>3</sub>)<sub>10</sub>, **12a**. (Stoichiometry of reactants are factored and mapped in all three schemes to get integral number for all products.)



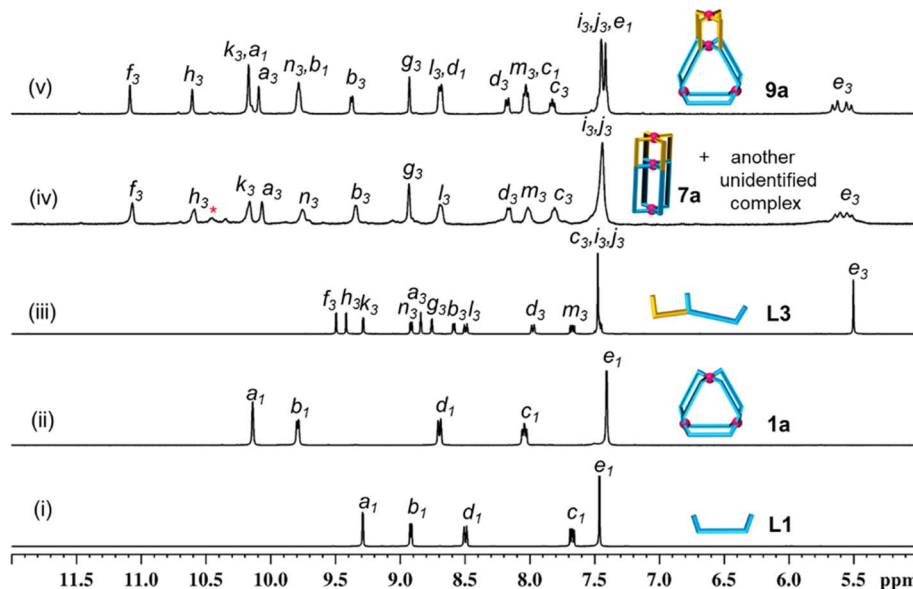


Fig. 3 Partial  $^1\text{H}$  NMR spectra (400 MHz,  $\text{DMSO-}d_6$ , 300 K) of (i) ligand **L1**; (ii)  $[\text{Pd}_3(\text{L1})_6](\text{NO}_3)_6$ , **1a**; (iii) ligand **L3**; (iv)  $[\text{Pd}_3(\text{L3})_4](\text{NO}_3)_6$ , **7a** (and another unidentified complex); and (v)  $[\text{Pd}_4(\text{L1})_2(\text{L3})_4](\text{NO}_3)_8$ , **9a**. Note: complex **9a** can be easily prepared from one-pot combination of  $\text{Pd}(\text{NO}_3)_2$ , **L1** and **L3** in a 4 : 2 : 4 ratio or cage fusion of **1a** with **7a** (and another unidentified complex) in a 1 : 3 ratio.

(1 mM and 30 mM of metal) (ESI Schemes S25–S27 $\dagger$ ) resulted in detectable amounts of  $\text{Pd}_2\text{L}_4$  and  $\text{Pd}_4\text{L}_8$  type complexes  $[\text{Pd}_2(\text{-L1}')_4](\text{NO}_3)_4$ , **2a'**, and  $[\text{Pd}_4(\text{L1}')_8](\text{NO}_3)_8$ , **3a'**, respectively, along with **1a'** as studied by  $^1\text{H}$  NMR spectroscopy and then confirmed by ESI-MS. $^{40}$  However, during the complexation of  $\text{Pd}(\text{NO}_3)_2$  with **L1**, no new complexes other than **1a** were observed at either lower or higher concentrations (1 mM or 30 mM of metal) in their  $^1\text{H}$  NMR spectra (ESI Fig. S53 $\dagger$ ). Incidentally,  $\text{Pd}_2\text{L}_4$  type  $[\text{Pd}_2(\text{L1})_4](\text{NO}_3)_4$ , **2a**, could be detected by ESI-MS (ESI Fig. S54 $\dagger$ ) but not  $\text{Pd}_4\text{L}_8$  type  $[\text{Pd}_4(\text{L1})_8](\text{NO}_3)_8$ , **3a**. Thus, the influence of concentration on nuclearity is neglected (as other complexes were not detected by NMR) for the complexation of  $\text{Pd}(\text{II})$  with **L1**. However, the presence of an undetectable amount of **3a** cannot be ruled out in the samples.

Complexation of  $\text{Pd}(\text{NO}_3)_2$  with the ligand **L2** also gave a  $\text{Pd}_3\text{L}_6$  type trinuclear complex  $[\text{Pd}_3(\text{L2})_6](\text{NO}_3)_6$ , **4a**, as shown in Scheme 1(ii) and ESI Scheme S10. $\dagger$   $^1\text{H}$  NMR spectral study (Fig. 4(i) and (ii)) revealed that the magnitude of downfield shift for inward- and outward-pointing  $\alpha$ -pyridine protons of **4a**, as compared to **L2** ( $\Delta\delta = 0.84$  and  $0.78$  ppm for  $\text{H}_{a2}$  and  $\text{H}_{b2}$ , respectively), is similar to that of **1a** as compared to **L1**. This is also true for  $\beta$ -/ $\gamma$ -pyridine protons. Concentration variation study (1 to 30 mM range) showed additional peaks at higher concentration in the  $^1\text{H}$  NMR spectra of the generated samples (ESI Fig. S60 $\dagger$ ). Since these peaks are negligible, we considered **4a** as an almost exclusive product in a range of concentrations.

As mentioned above, binuclear **2a** could be detected whereas tetranuclear **3a** could not be detected by ESI-MS during complexation study of **L1**. Thus for complexation of **L2** at lower concentration, we could not rule out the coexistence of **4a** along with undetectable amount of  $[\text{Pd}_2(\text{L2})_4](\text{NO}_3)_4$ , **5a**; but  $[\text{Pd}_4(\text{L2})_8](\text{NO}_3)_8$ , **6a**, might not coexist even at higher concentration. While ESI-MS study detected the presence of the usual

$\text{Pd}_3\text{L}_6$  type complex  $[\text{Pd}_3(\text{L2})_6](\text{BF}_4)_6$ , **4b**, only (ESI Fig. S61 $\dagger$ ), markedly binuclear **5a** (analogue of **2a**) and tetranuclear **6a** (analogue of **3a**) were not detected. Thus, the influence of concentration on the nuclearity is also ruled out for complexation of  $\text{Pd}(\text{II})$  with **L2**.

The complexes **1a** and **4a** were isolated in the solid state by a precipitation method using excess of EtOAc from their solutions in DMSO or  $\text{DMSO-}d_6$ .  $^1\text{H}$  NMR spectra of the isolated and *in situ* prepared complexes are found to be identical. The complexes **1a** and **4a** were characterized by ESI-MS and various NMR techniques including  $^1\text{H}$ ,  $^{13}\text{C}$ , H–H COSY, C–H COSY and H–H NOESY (ESI Fig. S47–S51 and S55–S59 $\dagger$ ). Gas-phase energy-minimized structures of the cationic part of the complexes **1a** and **4a** are shown in ESI Fig. S161. $\dagger$  The crystal structure of **1a** is also discussed in a later section. The metal centres in the complexes are located at the corners of an imaginary triangle where the calculated average non-bonded distances between two Pd centres in **1a** and **4a** are comparable (approximately 15 Å).

### Complexation of $\text{Pd}(\text{II})$ separately with unsymmetrical tris-monodentate ligands **L3** and **L4**

The ligand **L3** has a 3,5-disubstituted internal/central pyridine where the substituents are pyridine-appended arms of unequal lengths. The fragment spanning the length of the ligand from the internal/central pyridine to the pyridine of the shorter arm is known to form a  $\text{Pd}_2\text{L}_4$  type binuclear complex as reported earlier, $^{40}$  whereas the fragment comprising the internal/central pyridine which extends up to the pyridine unit of the longer arm (*i.e.* **L1**) forms a  $\text{Pd}_3\text{L}_6$  type complex as established in the present work. Self-assembly of  $\text{Pd}(\text{NO}_3)_2$  with the unsymmetrical tris-monodentate ligand **L3** was examined by combining them in a 3 : 4 ratio in  $\text{DMSO-}d_6$  at 70 °C (Scheme 1(iii), ESI Scheme S11 $\dagger$ ).



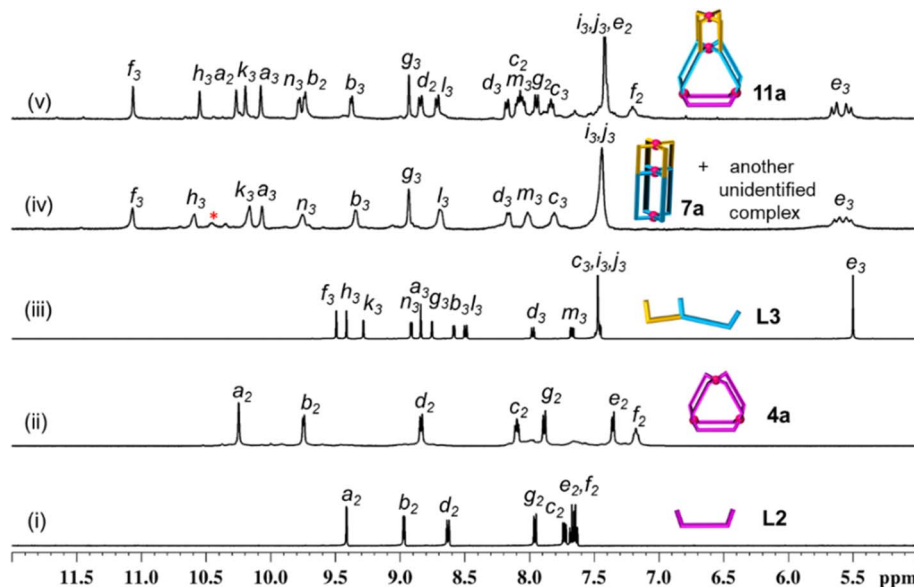


Fig. 4 Partial  $^1\text{H}$  NMR spectra (400 MHz,  $\text{DMSO}-d_6$ , 300 K) of (i) ligand **L2**; (ii)  $[\text{Pd}_3(\text{L2})_6](\text{NO}_3)_6$ , **4a**; (iii) ligand **L3**; (iv)  $[\text{Pd}_3(\text{L3})_4](\text{NO}_3)_6$ , **7a** (and another unidentified complex); and (v) low-symmetry  $[\text{Pd}_4(\text{L2})_2(\text{L3})_4](\text{NO}_3)_8$ , **11a**. (Note: complex **11a** can be easily prepared from one-pot combination of  $\text{Pd}(\text{NO}_3)_2$ , **L2** and **L3** in a 4 : 2 : 4 ratio or mixing **4a** and **7a** (and another unidentified complex) in a 1 : 3 ratio.)

The  $^1\text{H}$  NMR spectrum of the solution appeared like a single set of complexation-induced downfield shifted peaks, but slightly broad, when compared with free **L3** (Fig. 3(iii and iv)). Careful analysis indicated another set of overlapping signals (one of the peaks marked with an asterisk is not overlapped). Formation of double-cavity  $\text{Pd}_3\text{L}_4$  type  $[\text{Pd}_3(\text{L3})_4](\text{NO}_3)_6$ , **7a**, is identified by ESI-MS study (ESI Fig. S69 $^\dagger$ ) as one of the products. While DOSY NMR analysis showed the presence of two close-by bands where the major species is possibly **7a** (ESI Fig. S67 $^\dagger$ ) and we could not identify the other compound. In addition the possibility of  $\text{Pd}_6\text{L}_8$  type complex  $[\text{Pd}_6(\text{L3})_8](\text{NO}_3)_{12}$  cannot be ruled out (ESI Scheme S11 $^\dagger$ ). The  $^1\text{H}$  NMR peak pattern remained unchanged when the complexation reactions were performed at variable concentrations ranging from 2 to 40 mM with respect to metal (ESI Fig. S68 $^\dagger$ ). Incidentally, mixing of  $\text{Pd}(\text{NO}_3)_2$  with **L3'** (isomeric to **L3** having *meta*-phenylene spacer) is known to produce a mixture of double-cavity  $\text{Pd}_3\text{L}_4$  and triple-cavity  $\text{Pd}_6\text{L}_8$  type complexes  $[\text{Pd}_3(\text{L3}')_4](\text{NO}_3)_6$ , **7a'**, and  $[\text{Pd}_6(\text{L3}')_8](\text{NO}_3)_{12}$  (ESI Scheme S28 $^\dagger$ ). The mixture of **7a** and unidentified complex was characterized by recording  $^1\text{H}$ ,  $^{13}\text{C}$  NMR, H-H COSY, C-H COSY and H-H NOESY spectra (ESI Fig. S62–S66 $^\dagger$ ). Two unequal sized  $\text{Pd}_2\text{L}_4$  type cavities, conjoined with a common metal centre,<sup>40</sup> are present in the structure of the cage **7a** (as in **7a'**). The longer arm entity (see Fig. 2) of **L3** in its native form (*i.e.* **L1**) is ideal for making  $\text{Pd}_3\text{L}_6$  type arrangement (*i.e.* **1a**), but for **L3** as such this longer arm is not able to participate in  $\text{Pd}_3\text{L}_6$  formation due to the presence of a connected, binuclear cage forming, shorter arm entity. Thus, the longer arm in **L3** has two choices: to form (i) entropically unfavourable oligomerized products or (ii) entropically favourable but probably thermodynamically unfavourable discrete structures. Experimentally, the latter took place and **7a** was formed, but along with another unidentified compound (possibly  $\text{Pd}_6\text{L}_8$ ).

Similarly, complexation of  $\text{Pd}(\text{II})$  with **L4** resulted in a mixture of products (Scheme 1(iv), ESI Scheme S12 $^\dagger$ ) as suggested by the broad peaks and noisy baseline in the  $^1\text{H}$  NMR spectrum of the sample (ESI Fig. S70 and S71 $^\dagger$ ). The mixture might contain  $\text{Pd}_3\text{L}_4$  type complex  $[\text{Pd}_3(\text{L4})_4](\text{NO}_3)_6$ , **8a**, and other unidentified complexes probably including  $\text{Pd}_6\text{L}_8$  type cage. The DOSY NMR spectrum was collected for the reaction mixture which showed two nearby bands where major species could be **8a** (ESI Fig. S76 $^\dagger$ ). However, the presence of **8a** is indirectly inferred from the ESI-MS data that showed the existence of  $[\text{Cl} \leftarrow \text{Pd}_3(\text{L4})_4](\text{NO}_3)_5$ , **8ab** (ESI Fig. S77 $^\dagger$ ). The difference between the two related ligands **L3** and **L4** is evident in their spacer units that are 1,4-phenylene and naphthalene-1,5-diyl, respectively. This structural difference must be among the possible reasons for the variance in their complexation behaviours. Such a difference was not observed in the case of complexation of **L1** and **L2**; thus, the shorter arms of **L3** and **L4** also played some roles remotely.

#### One-pot complexation of $\text{Pd}(\text{II})$ with mixture of **L1** and **L3** (or mixture of **L2** and **L4**)

One-pot combination of  $\text{Pd}(\text{NO}_3)_2$  with a mixture of bis-monodentate ligand **L1** and tris-monodentate ligand **L3** was performed in a 4 : 2 : 4 ratio in anticipation of the tetranuclear mixed ligated cage  $[\text{Pd}_4(\text{L1})_2(\text{L3})_4](\text{NO}_3)_8$ , **9a** (Scheme 1(v), ESI Scheme S13 $^\dagger$ ) through integrative self-sorting.<sup>40</sup> The reaction was performed in  $\text{DMSO}-d_6$  at 70  $^\circ\text{C}$  and monitored by  $^1\text{H}$  NMR spectroscopy (ESI Fig. S78 $^\dagger$ ) to obtain a single set of sharp peaks within 2 h. Downfield shift of all the  $\alpha$ -pyridyl protons was observed in the  $^1\text{H}$  NMR spectrum of **9a** (Fig. 3(v)) as compared to the free ligands (six signals from **L3** and two from **L1**) indicating coordination of all pyridine moieties with  $\text{Pd}(\text{II})$ . For



bound **L3** units:  $\Delta\delta = 1.58, 1.18, 0.88, 1.25, 0.79$  and  $0.88$  ppm for  $H_{f3}, H_{h3}, H_{k3}, H_{a3}, H_{b3}$  and  $H_{n3}$ , respectively; and for bound **L1** units:  $\Delta\delta = 0.88$  and  $0.87$  for  $H_{k1}$  and  $H_{n1}$ , respectively. ESI-MS data of **9a** (ESI Fig. S85†) confirmed the proposed molecular formula. The success of integrative self-sorting is probably due to the unfavourable strain in one of the products (*i.e.* **7a**) if narcissistic self-sorting had occurred to produce **7a** and **1a**. The strain could be evaded when integratively self-sorted product **9a** was formed. In a similar fashion, complexation of  $\text{Pd}(\text{NO}_3)_2$  with a mixture of **L2** and **L4** produced integratively self-sorted product  $[\text{Pd}_4(\text{L2})_2(\text{L4})_4](\text{NO}_3)_8$ , **10a** (Scheme 1(vi), and ESI Scheme S14 and Fig. S86–S87†). The complexes **9a** and **10a** were obtained as single species confirmed by DOSY NMR (ESI Fig. S84 and S92†) and also further characterized by ESI-MS and various NMR techniques including  $^1\text{H}$ ,  $^{13}\text{C}$ , H–H COSY, C–H COSY and H–H NOESY (ESI Fig. S79–S83, S85 and S87–S91†). The complex **9a** was also characterized by the single-crystal XRD method as discussed in a later section.

### One-pot complexation of Pd(II) with mixture of L2 and L3 (or mixture of L1 and L4)

The calculated non-bonded distances between metal centres in the trinuclear complexes  $[\text{Pd}_3(\text{L1})_6](\text{NO}_3)_6$ , **1a**, and  $[\text{Pd}_3(\text{L2})_6](\text{NO}_3)_6$ , **4a**, are comparable (approximately  $15 \text{ \AA}$ ), as discussed above. Thus, it was proposed to prepare complexes like  $[\text{Pd}_4(\text{L2})_2(\text{L3})_4](\text{NO}_3)_8$ , **11a** (by one-pot combination of Pd(II), **L2** and **L3** in a 4 : 2 : 4 ratio) and  $[\text{Pd}_4(\text{L1})_2(\text{L4})_4](\text{NO}_3)_8$ , **12a** (by one-pot combination of Pd(II), **L1** and **L4** in a 4 : 2 : 4 ratio) (ESI Schemes S15 and S16†). In fact, the proposed complexes **11a** and **12a** could be easily prepared as shown in Scheme 1(xi) and (xii), by performing the reactions at  $70 \text{ }^\circ\text{C}$  in  $\text{DMSO-}d_6$ . The presence of a single band in DOSY NMR spectra revealed the formation of single discrete products **11a** and **12a** (ESI Fig. S100 and S108†). Further characterization was completed by various NMR techniques, namely  $^1\text{H}$ ,  $^{13}\text{C}$  NMR, H–H COSY, C–H COSY and H–H NOESY spectra (ESI Fig. S94–S99 and S102–S107†). ESI-MS data of both the complexes are given in ESI Fig. S101 and S109.†

The complexes **9a** and **10a** belong to a rare variety of tetranuclear complex of which only one example is known so far in the literature,<sup>40</sup> *i.e.*  $[\text{Pd}_4(\text{L1}')_2(\text{L3}')_4](\text{NO}_3)_8$ , **9a'** (ESI Scheme S29†). The complexes **11a** and **12a** are unusual as the longer arms in the trinuclear entity of **11a** (or **12a**) are unequal thus lowering the local symmetry at triangular builds, unlike the symmetrical triangular builds **9a'**, **9a**, and **10a**.

### Complexation of Pd(II) separately with symmetrical tris-monodentate ligands L5 and L6

The ligands **L5** and **L6** have a 3,5-disubstituted internal/central pyridine where the substituents are pyridine-appended arms of equal lengths for a given ligand. These arms of **L5** and **L6** along with the internal/central pyridine are essentially the ligands **L3** and **L4**, respectively. Thus, a question arises as to whether complexation of Pd(II) separately with the ligands **L5** and **L6** in a 3 : 4 ratio would result in double-cavity  $\text{Pd}_3\text{L}_4$  type complexes  $[\text{Pd}_3(\text{L5})_4](\text{NO}_3)_6$ , **13a**, and  $[\text{Pd}_3(\text{L6})_4](\text{NO}_3)_6$ , **14a**. In the case

where the strain is considerably high in the structure then the complexation of Pd(II) with **L5** (or **L6**) should possibly yield only oligomerized products, at the cost of discrete products.

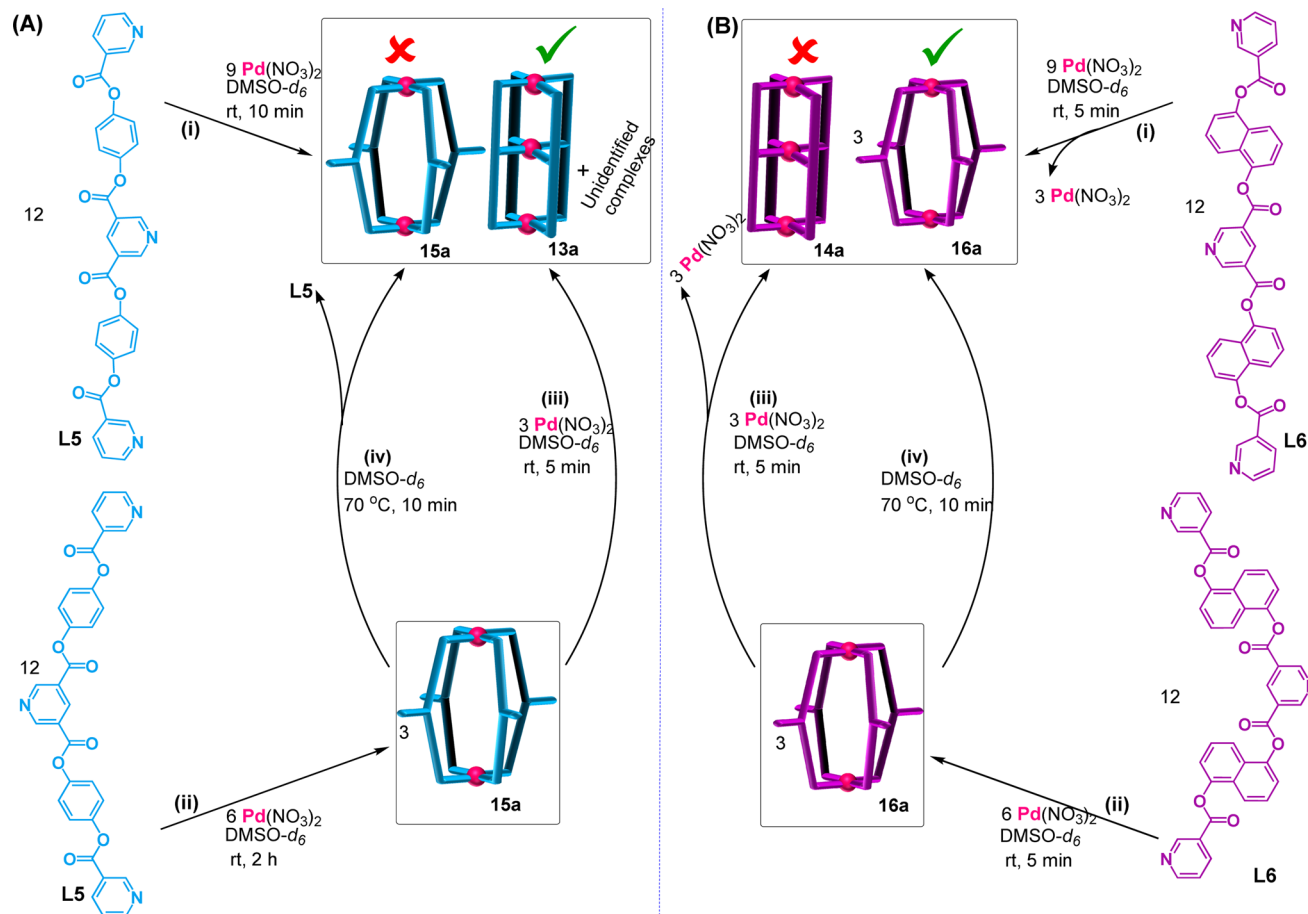
Keeping the above in mind,  $\text{Pd}(\text{NO}_3)_2$  was treated with ligand **L5** in a 3 : 4 ratio in  $\text{DMSO-}d_6$  (Scheme 2A(i), ESI Scheme S17†) and stirred at room temperature ( $27 \text{ }^\circ\text{C}$ ) whereupon a turbid reaction mixture was formed. The mixture was heated at  $70 \text{ }^\circ\text{C}$  for 10 min to get a clear solution and it was monitored by recording  $^1\text{H}$  NMR spectra as a function of time. At 10 min it showed broad unassignable signals (Fig. 5(ii)) and the peak pattern remained unchanged even after 48 h; thus, formation of a mixture of products was suspected as can be seen in the DOSY NMR spectrum (ESI Fig. S114†). ESI-MS study of the sample indicated the existence of **13a** as one of the products in the mixture though its proportion could not be ascertained from NMR study (ESI Fig. S110 and S115†).

Complexation of  $\text{Pd}(\text{NO}_3)_2$  with **L6** in  $\text{DMSO-}d_6$  was also performed in a 3 : 4 ratio (Scheme 2A(i), ESI Scheme S18†) whereupon a clear solution was obtained even at room temperature ( $27 \text{ }^\circ\text{C}$ ). Surprisingly, the  $^1\text{H}$  NMR spectrum recorded after 5 min of reaction time showed a single set of downfield-shifted and reasonably sharp signals (Fig. 5(v)). The simple nature of the NMR spectrum was a surprise to us as we did not expect to get the complex **14a** so easily (due to the inevitable strain expected from the naphthalene spacer). Careful analysis of the spectrum in comparison with that of the free ligand (Fig. 5(iv) and (v)) indicated that the terminal pyridine moieties of **L6** are coordinated with Pd(II) whereas the internal/central pyridine is uncoordinated; the protons of terminal pyridines are downfield shifted ( $\Delta\delta = 1.07$  and  $0.88$  ppm for  $H_{a6}$  and  $H_{b6}$ , respectively) and those of internal/central pyridine showed negligible but upfield shift. DOSY NMR verified the presence of single species (ESI Fig. S128†). This finding led us to believe that **14a** is not formed but that a binuclear  $\text{Pd}_2\text{L}_4$  type complex  $[\text{Pd}_2(\text{L6})_4](\text{NO}_3)_4$ , **16a**, is formed and one equivalent of Pd(II) per cage remained unutilized. This proposal of binuclear complex formation was confirmed by ESI-MS data of  $[\text{Pd}_2(\text{L6})_4](\text{BF}_4)_4$ , **16b** (ESI Fig. S129†). When the reaction was continued for a longer time, or even after heating at ( $70 \text{ }^\circ\text{C}$ ), no further changes were observed in the  $^1\text{H}$  NMR spectral peak pattern. The complex **16a** was characterized by  $^1\text{H}$ ,  $^{13}\text{C}$ , NMR, H–H COSY, C–H COSY and H–H NOESY (ESI Fig. S123–S127†).

Looking back at the already performed complexation of Pd(II) with **L5** in a 3 : 4 ratio that resulted in a mixture of products including trinuclear **13a**, it was decided to perform the reaction of Pd(II) with **L5** in a 2 : 4 ratio in  $\text{DMSO-}d_6$  (Scheme 2A(ii), ESI Scheme S19†). Interestingly, a clear solution was obtained within 2 h of reaction when carried out at room temperature. The  $^1\text{H}$  NMR spectrum of the solution showed a single set of sharp peaks (Fig. 5(iii)), the DOSY NMR spectrum showed a single band (ESI Fig. S121†) and ESI-MS confirmed the formation of  $\text{Pd}_2\text{L}_4$  type complex  $[\text{Pd}_2(\text{L5})_4](\text{NO}_3)_4$ , **15a** (ESI Fig. S122†). The complex **15a** remained stable in solution for at least 4 days, after which new broad peaks started appearing in the  $^1\text{H}$  NMR spectrum but **15a** still remained as major product (ESI Fig. S116†). The appearance of such new peaks was expediated upon heating the reaction solution at  $70 \text{ }^\circ\text{C}$ ; the complex







**Scheme 2** (A) (i)/(ii) Complexation of  $\text{Pd}(\text{NO}_3)_2$  with L5 in 3 : 4 and 2 : 4 ratios showing formation of **13a** and **15a**, respectively; (iii)/(iv) combination of **15a** with one equivalent of  $\text{Pd}(\text{NO}_3)_2$  per cage or simply heating at 70 °C, resulting in **13a**. (B) (i)/(ii) Complexation of  $\text{Pd}(\text{NO}_3)_2$  with L6 in 3 : 4 and 2 : 4 ratios showing formation of **16a** in both cases; (iii)/(iv) combination of **16a** with one equivalent of  $\text{Pd}(\text{II})$  per cage or simply heating at 70 °C resulting in no changes.

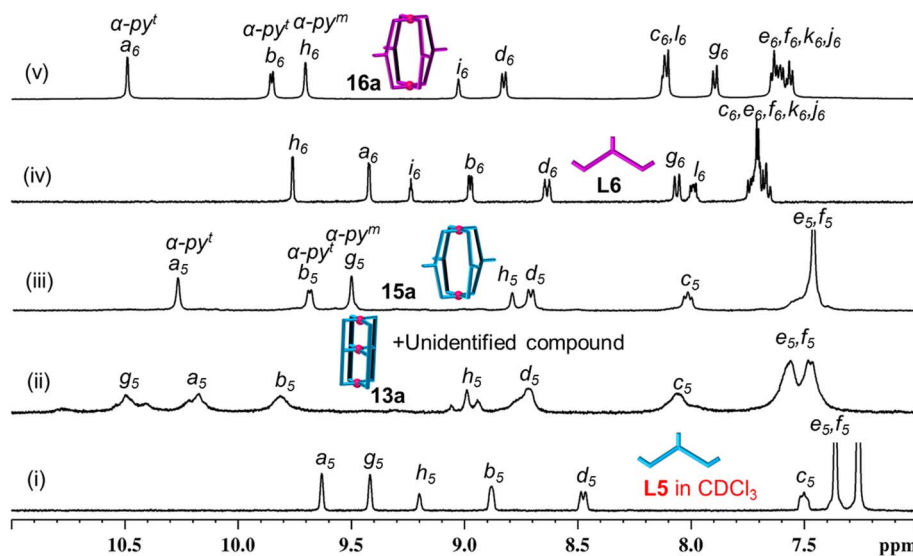
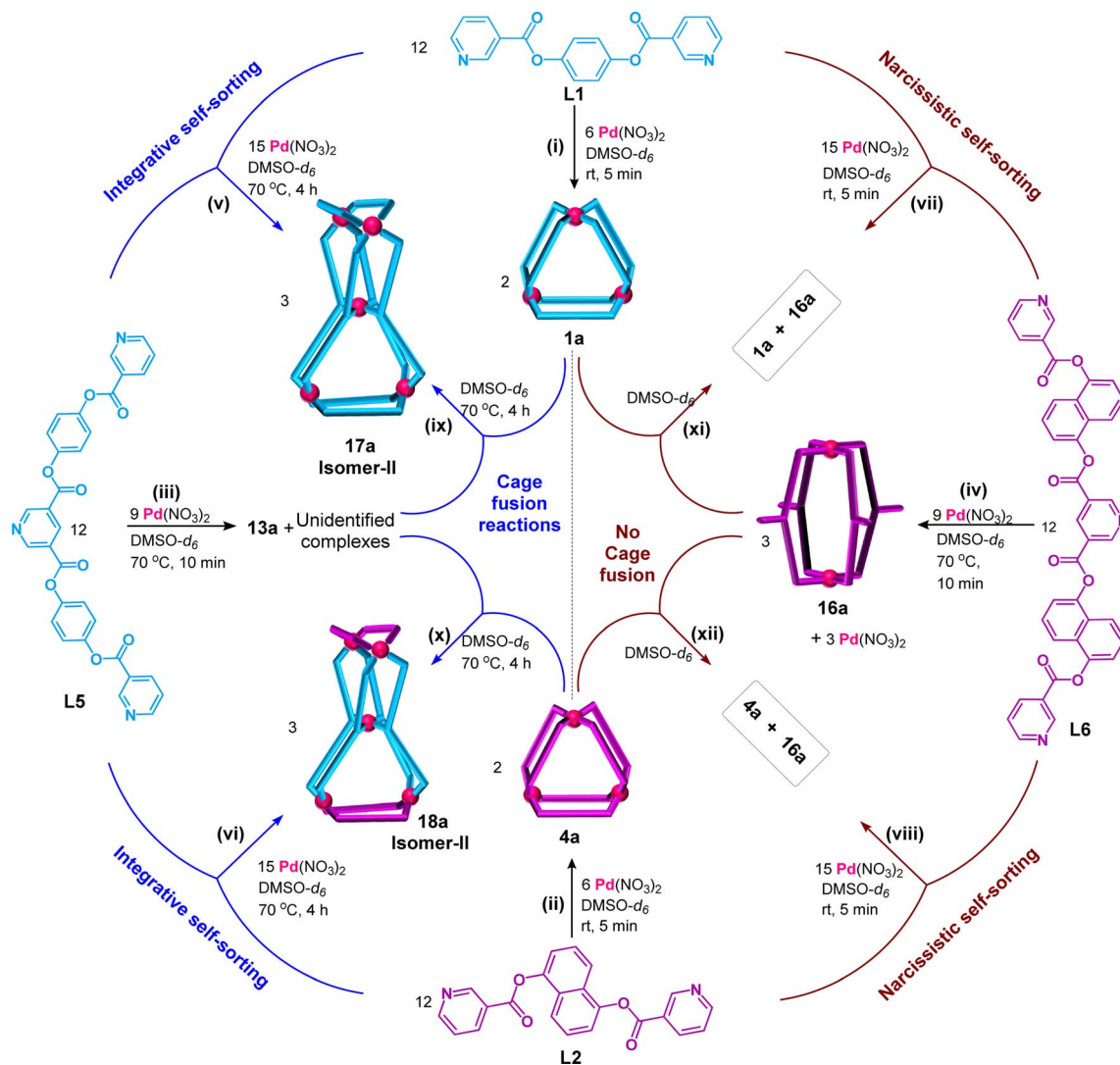


**Fig. 5** Partial  $^1\text{H}$  NMR spectra (400 MHz, DMSO- $d_6$ , 300 K) of (i) ligand L5 (in  $\text{CDCl}_3$ ); (ii)  $[\text{Pd}_3(\text{L5})_4](\text{NO}_3)_6$ , **13a**, and unidentified complexes; (iii)  $[\text{Pd}_2(\text{L5})_4](\text{NO}_3)_4$ , **15a**; (iv) ligand L6; and (v)  $[\text{Pd}_2(\text{L6})_4](\text{NO}_3)_4$ , **16a**. (Note: spectrum (ii) corresponds to complexation reaction of  $\text{Pd}(\text{II})$  with ligand L5 in 3 : 4 ratio.).





**Scheme 3** ((i)–(iv)) Complexation of  $\text{Pd}(\text{NO}_3)_2$  separately with ligands L1, L2, L5 and L6 giving **1a**, **4a**, **13a**, and **16a**, respectively; ((v) and (vi)) integrative self-sorting due to one-pot combination of  $\text{Pd}(\text{NO}_3)_2$ , L5 and L1 (or L2) resulting in isomer-II of  $[\text{Pd}_5(\text{L1})_4(\text{L5})_4](\text{NO}_3)_{10}$ , **17a** (or  $[\text{Pd}_5(\text{L2})_4(\text{L5})_4](\text{NO}_3)_{10}$ , **18a**); ((vii) and (viii)) narcissistic self-sorting due to one-pot combination of  $\text{Pd}(\text{NO}_3)_2$ , L6 and L1 (or L2) resulting in **1a** and **16a** (or **4a** and **16a**); ((ix) and (x)) cage fusion reactions of **13a** with **1a** (or **4a**) giving isomer-II of **17a** (or **18a**); ((xi) and (xii)) combination of **16a** with **1a** (or **4a**) in absence/presence of extra  $\text{Pd}(\text{NO}_3)_2$  resulting in no changes.

**15a** became a minor product within 10 min of heating (ESI Fig. S117†). The pattern of the new peaks resembled the pattern shown in Fig. 5(ii) corresponding to the sample obtained from one-step combination of  $\text{Pd}(\text{II})$  with L5 in a 3 : 4 ratio; the solution was turbid indicating dissociation of some amount of the ligands from the complex **15a** (Scheme 2A(iv)). Upon addition of another equivalent of  $\text{Pd}(\text{II})$  per cage of **15a** (*i.e.*  $\text{Pd}(\text{II})$  to L5 ratio was 3 : 4) (Scheme 2A(iii)), with or without heating, the peaks of binuclear **15a** completely disappeared and the spectrum resembled that shown in Fig. 5(ii). Thus, the unidentified products along with **13a** are anything but **15a**. The complex **15a** was characterized by  $^1\text{H}$  NMR, H–H COSY, and NOESY (ESI Fig. S118–S120†).

Subsequently, the complexation of  $\text{Pd}(\text{II})$  with L6 was performed in a 2 : 4 ratio (Scheme 2B(ii), ESI Scheme S20†) whereupon **16a** was formed as expected. Addition of another

equivalent of  $\text{Pd}(\text{II})$  to **16a** did not bring about any changes (Scheme 2B(iii)). The complex **16a** is considered to be quite stable as it remained unchanged after heating or after addition of another equivalent of  $\text{Pd}(\text{II})$ . However, the complex **15a** was found to be unstable as it rearranged giving a mixture, simply upon standing for few days at room temperature without requiring another equivalent of  $\text{Pd}(\text{II})$ . While the complex  $[\text{Pd}_3(\text{L5})_4](\text{NO}_3)_6$ , **13a**, was detected by ESI-MS, the complex  $[\text{Pd}_3(\text{L6})_4](\text{NO}_3)_6$ , **14a**, was not detected from complexation reactions of  $\text{Pd}(\text{II})$  with ligands at 3 : 4 ratios.

#### One-pot complexation of $\text{Pd}(\text{II})$ with mixture of L1 and L5 (or mixture of L2 and L5)

A mixture of  $\text{Pd}(\text{NO}_3)_2$ , L1 and L5 in a 5 : 4 : 4 ratio taken in  $\text{DMSO}-d_6$  (Scheme 3(v), ESI Scheme S21†) formed a suspension (as L5 is insoluble in  $\text{DMSO}$  medium). The suspension was



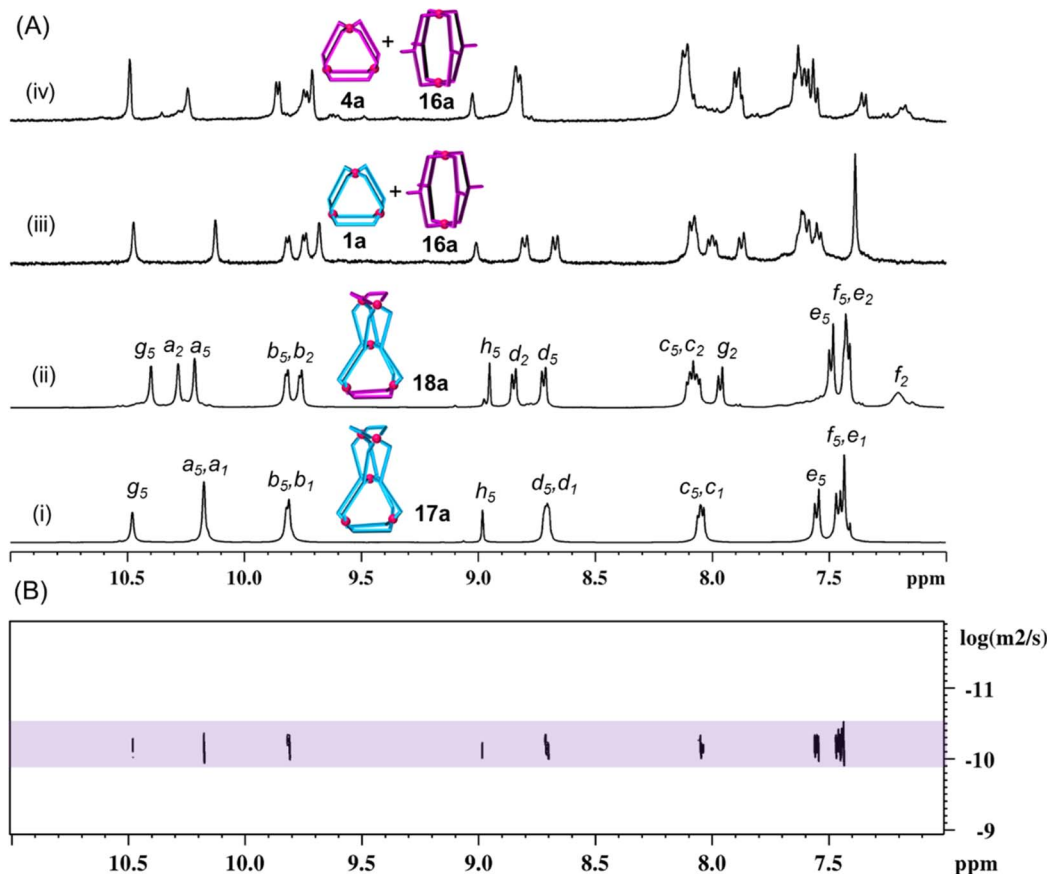


Fig. 6 (A) Partial  $^1\text{H}$  NMR spectra (400 MHz,  $\text{DMSO}-d_6$ , 300 K) of (i)  $[\text{Pd}_5(\text{L}1)_4(\text{L}5)_4](\text{NO}_3)_{10}$ , **17a**; (ii)  $[\text{Pd}_5(\text{L}2)_4(\text{L}5)_4](\text{NO}_3)_{10}$ , **18a**; (iii) mixture of **1a** and **16a**; (iv) mixture of **4a** and **16a**. (Note: the complexes are prepared from  $\text{Pd}(\text{II})$  and the relevant ligands taken in appropriate stoichiometries through (i)/(ii) integrative self-sorting and (iii)/(iv) narcissistic self-sorting.) (B)  $^1\text{H}$  DOSY NMR spectrum of complex **17a**.

stirred at room temperature (27 °C) and monitored by recording  $^1\text{H}$  NMR spectra as a function of time (ESI Fig. S130 $\dagger$ ). The spectrum recorded after 10 min showed only one set of sharp peaks corresponding to the formation of **1a** (due to interaction of  $\text{Pd}(\text{II})$  with **L1**) while **L5** was still insoluble. After 1 h of stirring, the peaks were slightly broadened and small humps also appeared around 10.5, 9.0 and 7.6 ppm due to partial dissolution of **L5** and thereby its participation in self-assembly processes, while the sample was still turbid. The turbidity disappeared gradually and humps turned to prominent peaks giving a single set of peaks (Fig. 6A(i)) after 4 days of stirring, indicating formation of a discrete product, thereafter no further changes were observed, suggesting completion of the reaction. When the reaction was carried out at 70 °C a clear solution was obtained within 4 h and the reaction was completed as confirmed by monitoring the reaction by the  $^1\text{H}$  NMR method (ESI Fig. S131 $\dagger$ ). We proposed the formation of our targeted single discrete product  $[\text{Pd}_5(\text{L}1)_4(\text{L}5)_4](\text{NO}_3)_{10}$ , **17a**, through integrative self-sorting which required 4 days at room temperature or 4 h at 70 °C. In the event of narcissistic self-sorting of  $\text{Pd}(\text{II})$ , **L1** and **L5** the formation of a mixture of products including **1a**, **13a** and unidentified complexes is conceivable, and broad signals in the  $^1\text{H}$  NMR spectrum (like Fig. 5(ii)), but that was not the case. Formation of a single species, *i.e.* **17a**, was

further supported by diffusion-ordered spectroscopy (DOSY), where the spectrum clearly showed a single band (Fig. 6(B), ESI Fig. S137 $\dagger$ ) with diffusion coefficient ( $D$ ) of  $6.45 \times 10^{-11} \text{ m}^2 \text{ s}^{-1}$ . Further, the molecular composition of **17a** was confirmed from ESI-MS data (ESI Fig. S138 $\dagger$ ).

For the complex **17a**, there should be two sets of terminal pyridine signals due to  $\text{H}_{a1}$ ,  $\text{H}_{b1}$ ,  $\text{H}_{c1}$  and  $\text{H}_{d1}$  (originated from bound **L1**) and  $\text{H}_{a5}$ ,  $\text{H}_{b5}$ ,  $\text{H}_{c5}$  and  $\text{H}_{d5}$  (originated from bound **L5**); four signals of one set are found to be overlapped with the signals of the other set. As expected, the positions of these signals are closely comparable with corresponding pyridine signals of **1a** as well as that of **13a**. Notably, for **17a** the chemical shift values of internal/central pyridine protons  $\text{H}_{g5}$  and  $\text{H}_{h5}$  (originated from bound **L5**) having sharp signals are also closely comparable to the corresponding signals of protons of **13a**, being broad signals. This is indicative of coordination of all pyridine units with  $\text{Pd}(\text{II})$  and the existence of a single product is already proposed above through DOSY. The use of the  $^1\text{H}$  NMR technique for calculation of complexation induced  $\Delta\delta$  values for **17a** as compared to **L5** moiety is not possible (due to solubility issues of **L5**), but  $\Delta\delta$  values with respect to **L1** moiety can be calculated easily and are found to be 0.88 and 0.89 ppm for  $\text{H}_{a1}$  and  $\text{H}_{b1}$ , respectively. The  $\text{H}_{g5}$  protons of **17a** are downfield shifted by 0.97 ppm as compared to the  $\text{H}_{g5}$  protons of **15a** (in



**15a** the central pyridine of **L5** is not coordinated with a metal centre). This comparison is an additional support for claiming the coordination of internal/central pyridine in **17a**. Characterization of **17a** was also carried out by NMR techniques including  $^1\text{H}$ ,  $^{13}\text{C}$ , H–H COSY, C–H COSY and H–H NOESY (ESI Fig. S132–S136†).

Preparation of the tetranuclear  $[\text{Pd}_4(\text{L1})_2(\text{L3})_4](\text{NO}_3)_8$ , **9a**, and a lower symmetry tetranuclear  $[\text{Pd}_4(\text{L2})_2(\text{L3})_4](\text{NO}_3)_8$ , **11a**, by integrative self-sorting is described in the previous sections. In a similar line and taking inspiration from the synthesis of pentanuclear **17a** we targeted the lower symmetry pentanuclear complex  $[\text{Pd}_5(\text{L2})_4(\text{L5})_4](\text{NO}_3)_{10}$ , **18a**. The complex **18a** was prepared through integrative self-sorting of  $\text{Pd}(\text{NO}_3)_2$ , **L2** and **L5** in a 5 : 4 : 4 ratio taken in  $\text{DMSO}-d_6$  (Scheme 3(vi), ESI Scheme S22†) which required stirring for 4 days at room temperature or 4 h at 70 °C. A single set of sharp peaks (Fig. 6A(ii)) with well separated and assignable signals in the  $^1\text{H}$  NMR spectrum, a single band with a diffusion coefficient of  $6.3 \times 10^{-11} \text{ m}^2 \text{ s}^{-1}$  (ESI Fig. S144†) and convincing ESI-MS data provided enough support for the formation of single discrete structure **18a** (ESI Fig. S145†). The complete characterization of complex **18a** was done by NMR techniques including  $^1\text{H}$ ,  $^{13}\text{C}$ , H–H COSY, C–H COSY and H–H NOESY (ESI Fig. S139–S143†).

Two isomeric arrangements, *i.e.* planar isomer-I and orthogonal isomer-II, are conceivable for the three-dimensional structures of **17a** and **18a**. The structure determined using single-crystal X-ray diffraction data corresponded with isomer-II for **18a** (discussed in a later section), whereas we were not successful in growing single crystals of **17a** after several trials. DFT calculation (discussed in a later section) supported energetic preference for isomer-II for both the complexes. Hence, formation of isomer-II is also proposed for the complex **17a**. Isomers I and II of a given cage have different bonding patterns with respect to metal-to-ligand bonds; these are not conformers of each other. In isomer-I it is possible to locate a pair of tris-monodentate ligands completely describing an edge of one triangle and an edge of another triangle, whereas in isomer-II this is not so. A pair of tris-monodentate ligands in isomer-II completely describe the edge of only one of the triangles and partially describe two edges of another triangle. In the planar isomer-I, both of the triangular moieties are portrayed to be located almost on the same plane, whereas in the orthogonal isomer-II the triangles are orthogonally placed with respect to each other.

### One-pot complexation of Pd(II) with mixture of L2 and L6 (or mixture of L1 and L6)

Detailed investigation indicated that the internal/central pyridine of **L6** is unsuitable for coordination with  $\text{Pd}(\text{II})$ . Therefore it is not expected to afford pentanuclear complexes like  $[\text{Pd}_5(\text{L2})_4(\text{L6})_4](\text{NO}_3)_{10}$ , **19a**, and  $[\text{Pd}_5(\text{L1})_4(\text{L6})_4](\text{NO}_3)_{10}$ , **20a**. Nevertheless, complexation reactions were tried by combining  $\text{Pd}(\text{NO}_3)_2$ , **L2**, and **L6** in a 5 : 4 : 4 ratio in  $\text{DMSO}-d_6$  (Scheme 3(viii), ESI Scheme S23†). Unsurprisingly, narcissistic self-sorting was observed spontaneously at room temperature (27 °C) resulting in a mixture of  $[\text{Pd}_3(\text{L2})_6](\text{NO}_3)_6$ , **4a**, and  $[\text{Pd}_2(\text{L6})_4](\text{NO}_3)_4$ , **16a**, as confirmed by monitoring the reaction

by  $^1\text{H}$  NMR spectroscopy (Fig. 6A(iv)). Longer reaction time and heating at 70 °C did not bring about any change to the product profile. In a similar line combination of  $\text{Pd}(\text{NO}_3)_2$ , **L1**, and **L6** in a 5 : 4 : 4 ratio in  $\text{DMSO}-d_6$  (Scheme 3(vii), Fig. 6A(iii), ESI Scheme S24†) also exhibited narcissistic self-sorting to produce  $[\text{Pd}_3(\text{L1})_6](\text{NO}_3)_6$ , **1a**, and  $[\text{Pd}_2(\text{L6})_4](\text{NO}_3)_4$ , **16a**. It is assumed that unfavourable strain hindered the formation of the imaginary molecules **19a** and **20a**.  $^1\text{H}$  NMR spectra of relevant ligands and complexes are plotted together for a quick reference and comparison (ESI Fig. S146 and S147†).

### Cage fusion reactions

The tetranuclear complexes (**9a**, **10a**, **11a**, and **12a**) and pentanuclear complexes (**17a** and **18a**) prepared in the present work were exclusively formed by integrative self-sorting of  $\text{Pd}(\text{II})$  and a pair of appropriate ligands (**L1** to **L6**). We considered a library of complexes (**1a**, **4a**, **7a**, **8a**, **13a**, and **16a**) prepared from  $\text{Pd}(\text{II})$  and individual ligands. Understandably, combination of two selected complexes/cages from the library would essentially undergo cage fusion reactions leading to the integratively self-sorted tetra- and pentanuclear complexes cited above. For instance, complexation of  $\text{Pd}(\text{II})$  with **L1** and **L3** separately results in cages  $[\text{Pd}_3(\text{L1})_6](\text{NO}_3)_6$ , **1a**, and  $[\text{Pd}_3(\text{L3})_4](\text{NO}_3)_6$ , **7a**, respectively, whereas one-pot mixing of  $\text{Pd}(\text{II})$ , **L1** and **L3** produces cage  $[\text{Pd}_4(\text{L1})_2(\text{L3})_4](\text{NO}_3)_8$ , **9a**. For the cage fusion reaction, cages **1a** and **7a** were combined in a 1 : 3 ratio whereupon three equivalents of **9a** were generated exclusively (Scheme 1(ix)). Cage fusion reactions were successfully performed for all other complexes that are formed by integrative self-sorting processes (Schemes 1(x)–(xii) and 3(ix) and (x)). The progress of the cage fusion reactions generating **9a** was monitored by  $^1\text{H}$  NMR spectroscopy for a better evaluation (ESI Fig. S148†). Similarly, the progress of the reaction for other cage fusion reactions was also monitored (ESI Fig. S149–S151 and S152–S155†). It is well known that thermodynamic stability drives the formation of integratively self-sorted products in contrast to narcissistically sorted products. In the present work, we believe that thermodynamic stability is the reason for the formation of pentanuclear mixed-ligated double-cavity cages **17a** and **18a**.

A mixture of complexes **1a** and **16a** was formed by narcissistic self-sorting using  $\text{Pd}(\text{II})$ , **L1** and **L6**. Obviously, combination of isolated **1a** and **16a** would not undergo cage fusion and that was the case (Scheme 3(vii), ESI Fig. S156†). Similarly, a mixture of **4a** and **16a** also remained intact and there was no cage fusion (Scheme 3(viii), ESI Fig. S157†).

### Single-crystal X-ray diffraction analysis

Structures of  $[\text{Pd}_3(\text{L1})_6](\text{NO}_3)_6$ , **1a**,  $[\text{Pd}_4(\text{L1})_2(\text{L3})_4](\text{NO}_3)_8$ , **9a**, and  $[\text{Pd}_5(\text{L2})_4(\text{L5})_4](\text{NO}_3)_{10}$ , **18a**, are unequivocally confirmed by single-crystal X-ray diffraction study. The structures are shown in Fig. 7 and a brief description is given below. Further description about the crystallographic data, structural refinement and ORTEP diagrams are provided in the ESI (Table S1 and Fig. S158–S160†).



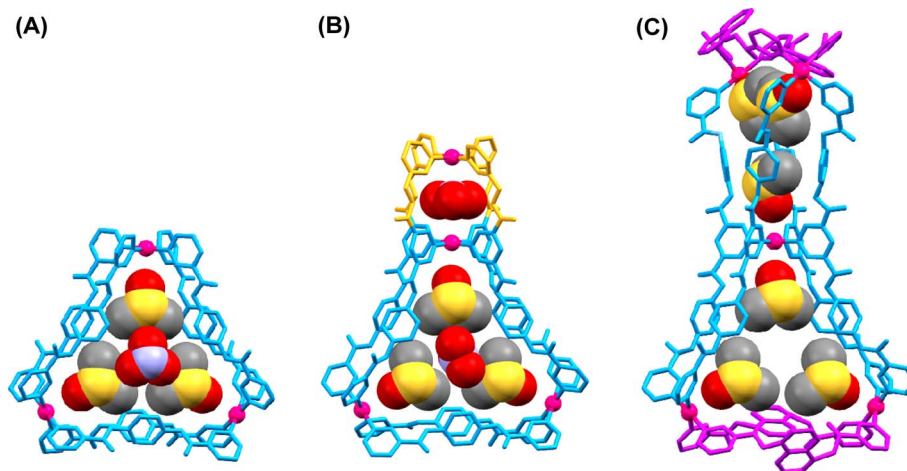


Fig. 7 Crystal structures showing cationic frameworks and encapsulated solvents/counter-anions corresponding to the cages (A) **1a**, (B) **9a**, and (C) **18a**.

**Trinuclear complex 1a.** Crystals of complex **1a** were obtained by slow diffusion of  $\text{CCl}_4$  vapour into a DMSO solution of  $[\text{Pd}_3(\text{L1})_6](\text{NO}_3)_6$ , **1a**. Structure solution using single-crystal X-ray diffraction data revealed that the complex **1a** crystallizes in the trigonal space group  $P\bar{3}1c$  with one  $\text{Pd}(\text{II})$  center and two ligands in the asymmetric unit. The asymmetric unit also contains four  $\text{CCl}_4$  and five DMSO molecules along with nitrate ions. The electron density corresponding to other disordered solvent molecules was squeezed. The  $\text{Pd}(\text{II})$  centres lie at the vertices of an imaginary equilateral triangle, separated by a distance of  $14.865(2)$  Å. The carbonyl groups of the ester ligand point outside the cavity and are involved in weak, non-covalent interactions with solvent molecules. Three DMSO molecules located inside the cage cavity engage in C–H...O interactions with a single nitrate anion present on the central inner surface of the triangular cavity.

**Tetranuclear complex 9a.** Crystals of complex **9a** were obtained by slow diffusion of toluene vapour into a DMSO solution of  $[\text{Pd}_4(\text{L1})_2(\text{L3})_4](\text{NO}_3)_8$ . The complex **9a** crystallizes in the triclinic space group  $P\bar{1}$  with one molecule of the tetranuclear complex, eight nitrate ions and six DMSO molecules in the asymmetric unit. The electron density corresponding to other disordered solvent molecules was squeezed. The small cavity houses a single nitrate anion which is involved in C–H...O contacts with the pyridyl protons of the ligand. Three DMSO solvent molecules are present in the larger cavity. A second nitrate ion is also present in the central portion of the triangular cavity and interacts with the DMSO molecules *via* noncovalent interactions.

**Pentanuclear complex 18a.** Crystals of complex **18a** were obtained by slow diffusion (over a period of two weeks) of toluene vapour into a DMSO solution of  $[\text{Pd}_5(\text{L2})_4(\text{L5})_4](\text{NO}_3)_{10}$ . The complex **18a** crystallizes in the tetragonal non-centrosymmetric space group  $P4_22_12$  with one half molecule of the pentanuclear complex, five nitrate ions and three DMSO molecules in the asymmetric unit. The electron density corresponding to other disordered solvent molecules was squeezed. The novel pentanuclear complex is formed by a pair of

conjoined trinuclear cages which share a  $\text{Pd}(\text{II})$  centre. The dihedral angle between the two planes defined by the three  $\text{Pd}(\text{II})$  centres ( $\text{Pd}2$  is common to both cages) of the conjoined trinuclear cages is  $87.71^\circ$ . Each cavity contains three DMSO molecules and the anions are present outside these cavities.

#### DFT study to comprehend bend angle of free and bound ligands

Non-chelating bis-monodentate ligands are known to form  $\text{Pd}_n\text{L}_{2n}$  types of complexes where the value of “ $n$ ” is related to the bend angle ( $\theta$ ) of the coordination vectors of bound-ligand units. For binuclear  $\text{Pd}_2\text{L}_4$  and hexanuclear  $\text{Pd}_6\text{L}_{12}$  type complexes having the metal ions arranged at the end of a line and the vertices of an octahedron, the ideal values of  $\theta$  are  $0^\circ$  and  $90^\circ$ , respectively.<sup>12,46</sup> In such cases, the square planar coordination geometry around the metal centre is either maintained or shows a small deviation. For ring-like trinuclear  $\text{Pd}_3\text{L}_6$ , tetranuclear  $\text{Pd}_4\text{L}_8$  and pentanuclear  $\text{Pd}_5\text{L}_{10}$  type complexes the values of  $\theta$  are below  $90^\circ$ .<sup>12</sup> The values of  $\theta$  calculated from the crystal structures of a few reported systems are approximately  $0^\circ$  for  $\text{Pd}_2\text{L}_4$  type complexes and in the range of  $40^\circ$  to  $50^\circ$  for  $\text{Pd}_3\text{L}_6$  type complexes. If the bend angle of free ligand (in one of the stable conformers) is comparable/matching with the required bend angle of the bound ligand in a  $\text{Pd}_n\text{L}_{2n}$  type complex then we can expect the formation of such a complex if  $\text{Pd}(\text{II})$  is combined with the ligand. The strain imposed in the overall structure of the coordination architecture should be within the limit of tolerance whenever the bend angles match.

Keeping this in mind, energy-minimized structures of the free ligands (**L1–L6**) and the cationic frameworks of a range of the  $\text{Pd}(\text{II})$  complexes of the ligands, including mixed ligated complexes, were obtained by the density functional theory (DFT) method (ESI Fig. S161–S163†). The bend angles of the free ligands and bound ligands are estimated in order to qualitatively understand whether or not considerable strain is imposed on the ligand backbone of some of the coordination



architectures (ESI Fig. S161–S163†). The calculated bend angles of ligands **L1** and **L2** are found to be suitable for supporting  $\text{Pd}_3\text{L}_6$  architecture (as in **1a** and **4a**); the longer arms of the ligands **L3** and **L4** are also suitable for  $\text{Pd}_3\text{L}_6$  sub-framework but participation of either **L1** or **L2** as ancillary ligand is required (as in **9a** to **12a**) for making a discrete structure.

The arms of ligand **L5** are well suited for the making of  $\text{Pd}_3\text{L}_6$  fragments but by including either **L1** or **L2** as ancillary ligand (as in **17a** and **18a**). In the absence of ancillary ligand, the ligand **L5** is forced to support  $\text{Pd}_2\text{L}_4$  sub-framework (as in **13a**) of a  $\text{Pd}_3\text{L}_4$  cage. The ligand **L6** could not support  $\text{Pd}_3\text{L}_4$  (as in imaginary **14a**); also, even in the presence of ancillary ligand it did not support  $\text{Pd}_3\text{L}_6$  sub-frameworks (as in imaginary **19a** and **20a**) due to formation of alternate stable structure, *i.e.* **16a** where bend angle is not an issue.

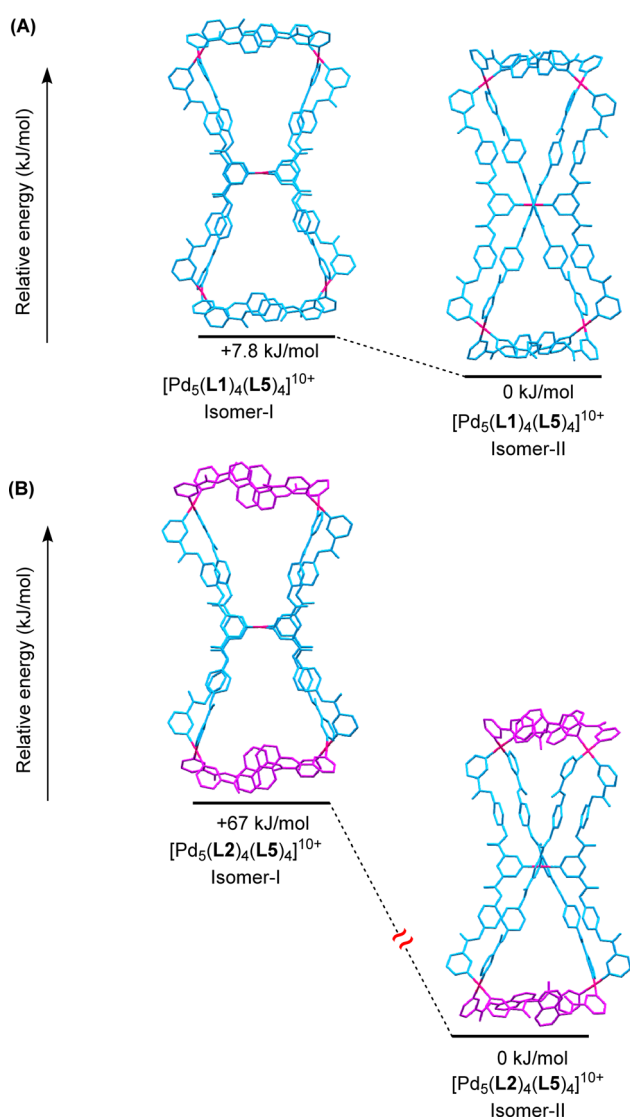


Fig. 8 Energy-minimized structures (B3LYP-D3/SDD,6-31G(d)) showing energetic preference between planarly conjoined (isomer-I) and orthogonally conjoined (isomer-II) triangles for (A)  $[\text{Pd}_5(\text{L1})_4(\text{L5})_4]^{10+}$ , **17a**, and (B)  $[\text{Pd}_5(\text{L2})_4(\text{L5})_4]^{10+}$ , **18a**, in the gas phase. (Hydrogen atoms are omitted for clarity; counter-anions/solvents were not included in the calculations.)

### DFT study on planarly/orthogonally conjoined triangles

DFT calculations were performed to find out whether the structure of isomer-II obtained from single-crystal X-ray diffraction data is energetically preferred over isomer-I for the cationic framework  $[\text{Pd}_5(\text{L2})_4(\text{L5})_4]^{10+}$  of the pentanuclear complex **18a**. The gas-phase calculations (ESI Tables S8 and S9†) showed that the isomer-II, *i.e.* **18a-II**, is considerably preferred (by 67 kJ mol<sup>-1</sup>) as compared to **18a-I** (Fig. 8(B)). Similar calculations for the two isomers of the cationic framework  $[\text{Pd}_5(\text{L1})_4(\text{L5})_4]^{10+}$  of the pentanuclear complex **17a** in the gas phase revealed that **17a-II** is preferred (by 7.8 kJ mol<sup>-1</sup>) over **17a-I** (Fig. 8(A)). Various views of both the isomers of the complexes **17a** and **18a** are shown in ESI Fig. S164–S167,† for better three-dimensional visualization. However, energy optimization of the complexes **17a** and **18a** in implicit DMSO was not successful. In isomer-I, both of the triangular moieties appear to be located on the same plane, whereas in the orthogonal isomer-II the triangles are orthogonally placed with respect to each other. The planar isomer-I was found to be not completely planar in the DFT structure. A triangle is slightly twisted from the plane of the other and the square planar nature of Pd(II) centres is also disturbed making isomer-I less preferred.

## 3 Conclusions

In summary, we have carefully designed a set of symmetrical bis-monodentate (**L1**), unsymmetrical tris-monodentate (**L3**) and symmetrical tris-monodentate (**L5**) ligands. Complexation of Pd(II) with the individual ligands **L1**, **L3** and **L5** resulted in relaxed  $[\text{Pd}_3(\text{L1})_6]^{6+}$  (exclusively),  $[\text{Pd}_3(\text{L3})_4]^{6+}$  (almost exclusively), and  $[\text{Pd}_3(\text{L5})_4]^{6+}$  (in a mixture). This complexation behaviour provided a basis for the targeted mixed-ligated MCDCC. Complexation of Pd(II) with a mixture of **L1** and **L3** in a 4 : 2 : 4 ratio resulted in integrative self-sorting to form a relaxed double-cavity  $[\text{Pd}_4(\text{L1})_2(\text{L3})_4]^{8+}$  framework containing binuclear and trinuclear sub-frameworks that are conjoined at a common metal centre. Integrative self-sorting of Pd(II), **L1** and **L5** in a 5 : 4 : 4 ratio resulted in the relaxed double-cavity  $[\text{Pd}_5(\text{L1})_4(\text{L5})_4]^{10+}$  framework where two trinuclear sub-frameworks are conjoined. The complexation behaviour of another set of ligands **L2**, **L4** and **L6** that are comparable to **L1**, **L3** and **L5** was also studied. The tris-monodentate ligand **L6** behaved very differently from **L5** in that complexation of Pd(II) with **L6** resulted in a stable binuclear single-cavity complex  $[\text{Pd}_2(\text{L6})_4]^{4+}$ . Integrative self-sorting was observed for the combination of Pd(II), **L2** and **L4** in a 4 : 2 : 4 ratio resulting in  $[\text{Pd}_4(\text{L2})_2(\text{L4})_4]^{8+}$  whereas narcissistic self-sorting was observed for the combination of Pd(II), **L2** and **L6** resulting in the individual complexes  $[\text{Pd}_3(\text{L2})_6]^{6+}$  and  $[\text{Pd}_2(\text{L6})_4]^{4+}$ . The success of the observed integrative self-sorting is ascribed to two factors, *i.e.* (i) size complementarity of the two ligands in the targeted design and (ii) strained/oligomeric complexes formed by at least one of the ligands. Lowering the symmetry of multi-cavity complexes was achieved by integrative self-sorting leading to exclusive formation of  $[\text{Pd}_4(\text{L2})_2(\text{L3})_4]^{8+}$ ,  $[\text{Pd}_4(\text{L1})_2(\text{L4})_4]^{8+}$  and  $[\text{Pd}_5(\text{L2})_4(\text{L5})_4]^{10+}$ . However, we did not expect the formation of  $[\text{Pd}_5(\text{L1})_4(\text{L6})_4]^{10+}$ , and it did not form.



Devising methods for lowering the symmetry of SCDCC is a relatively new research area; here we have gone a step further and demonstrated a strategy to lower the symmetry in MCDCC. Our work provided design principles for the construction of a new and novel pentanuclear double-cavity framework composed of two trinuclear sub-frameworks. We recommend the following two points for selection of bis-monodentate and tris-monodentate ligands for preparation of new pentanuclear MCDCC. (1) It is crucial to select a bis-monodentate ligand that is capable of forming a relaxed trinuclear complex upon complexation with Pd(II). (2) It is necessary to prepare a tris-monodentate ligand that resembles two units of the bis-monodentate ligand having a common donor site and then evaluate the complexation behaviour of Pd(II) with the tris-monodentate ligand; select those ligands that yield strained complexes or oligomers and reject those that form stable complexes. The pentanuclear MCDCC design introduced by us should inspire the making of many more such complexes by variation of spacer in the ligands to modulate the shapes, sizes and ultimately the behaviour/reactivity aspects of MCDCC.

## Data availability

All relevant data have been included in the paper and ESI.†

## Author contributions

D. K. C. and S. S. carried out the research, analyzed the data and wrote the manuscript. S. P. synthesized and characterized the complexes **1a** and **4a**; S. S. took over the work from S. P. to proceed further with the synthesis of ligands, complexation study, growing of all crystals, and computational study. S. P. helped in scientific discussion. S. K. carried out X-ray diffraction experiments and refined two crystal structures and contributed to the manuscript preparation. D. K. C. is the principal investigator and managed the project.

## Conflicts of interest

There are no conflicts to declare.

## Acknowledgements

D. K. C. thanks the Science and Engineering Research Board (SERB), Department of Science and Technology, Government of India (project no. CRG/2022/004413), for financial support. D. K. C. thanks IIT Madras for financial support through a Mid-Career Institute Research and Development Award (IRDA-2019) and through a Center under Institute of Eminence program (IoE Center of Molecular Architecture). We thank SAIF, IIT Madras for single-crystal XRD facility (especially Dr P. K. S. Antharjanam for refining crystal structure of **9a**). We thank the Department of Chemistry, IIT Madras, for NMR facility (especially Dr R. Baskar for helping in DOSY NMR study), and DST-FIST funded ESI-MS facility. We thank the P. G. Senapathy Centre for Computing Resources, IIT Madras, for providing access to the Gaussian16 package. S. S. thanks IIT Madras for

a fellowship. S. P. thanks CSIR, New Delhi, India for a fellowship. This Edge Article is dedicated to Prof. Ashok K. Mishra on the occasion of his superannuation.

## References

- M. M. J. Smulders, I. A. Riddell, C. Browne and J. R. Nitschke, *Chem. Soc. Rev.*, 2013, **42**, 1728–1754.
- T. R. Cook and P. J. Stang, *Chem. Rev.*, 2015, **115**, 7001–7045.
- M. Yoshizawa, *Chem. Lett.*, 2017, **46**, 163–167.
- N. B. Debata, D. Tripathy and H. S. Sahoo, *Coord. Chem. Rev.*, 2019, **387**, 273–298.
- E. Raee, Y. Q. Yang and T. B. Liu, *Giant*, 2021, **5**, 100050.
- A. J. McConnell, *Chem. Soc. Rev.*, 2022, **51**, 2957–2971.
- A. Tarzia and K. E. Jelfs, *Chem. Commun.*, 2022, **58**, 3717–3730.
- Y. Domoto and M. Fujita, *Coord. Chem. Rev.*, 2022, **466**, 214605.
- T. Tateishi, M. Yoshimura, S. Tokuda, F. Matsuda, D. Fujita and S. Furukawa, *Coord. Chem. Rev.*, 2022, **467**, 214612.
- K. Harris, D. Fujita and M. Fujita, *Chem. Commun.*, 2013, **49**, 6703–6712.
- M. Han, D. M. Engelhard and G. H. Clever, *Chem. Soc. Rev.*, 2014, **43**, 1848–1860.
- S. Saha, I. Regeni and G. H. Clever, *Coord. Chem. Rev.*, 2018, **374**, 1–14.
- J. E. M. Lewis, *Chem. Commun.*, 2022, **58**, 13873–13886.
- S. Sharma, M. Sarkar and D. K. Chand, *Chem. Commun.*, 2023, **59**, 535–554.
- A. Schmidt, A. Casini and F. E. Kuhn, *Coord. Chem. Rev.*, 2014, **275**, 19–36.
- J. E. M. Lewis and J. D. Crowley, *ChemPlusChem*, 2020, **85**, 815–827.
- D. Tripathy, N. B. Debata, K. C. Naik and H. S. Sahoo, *Coord. Chem. Rev.*, 2022, **456**, 214396.
- S. S. Mishra and D. K. Chand, *Dalton Trans.*, 2022, **51**, 11650–11657.
- R.-J. Li, A. Tarzia, V. Posligua, K. E. Jelfs, N. Sanchez, A. Marcus, A. Baksi, G. H. Clever, F. F. Tirani and K. Severin, *Chem. Sci.*, 2022, **13**, 11912–11917.
- P. Molinska, A. Tarzia, L. Male, K. E. Jelfs and J. E. M. Lewis, *Angew. Chem., Int. Ed.*, 2023, **62**, e202315451.
- J. D. Montmollin, A. B. Solea, D. W. Chen, F. F. Tirani and K. Severin, *Inorg. Chem.*, 2024, **63**, 4583–4588.
- W. M. Bloch and G. H. Clever, *Chem. Commun.*, 2017, **53**, 8506–8516.
- S. Pullen and G. H. Clever, *Acc. Chem. Res.*, 2018, **51**, 3052–3064.
- D. Bardhan and D. K. Chand, *Chem.–Eur. J.*, 2019, **25**, 12241–12269.
- J. L. Algar and D. Preston, *Chem. Commun.*, 2022, **58**, 11637–11648.
- C.-B. Tian and Q.-F. Sun, *Chem.–Eur. J.*, 2023, **29**, e202300195.
- R. A. S. Vasdev, D. Preston and J. D. Crowley, *Chem.–Asian J.*, 2017, **12**, 2513–2523.



- 28 S. Pullen, J. Tessarolo and G. H. Clever, *Chem. Sci.*, 2021, **12**, 7269–7293.
- 29 C. T. McTernan, J. A. Davies and J. R. Nitschke, *Chem. Rev.*, 2022, **122**, 10393–10437.
- 30 H. Furukawa, K. E. Cordova, M. O’Keeffe and O. M. Yaghi, *Science*, 2013, **341**, 1230444.
- 31 J. H. Lee, S. Jeoung, Y. G. Chung and H. R. Moon, *Coord. Chem. Rev.*, 2019, **389**, 161–188.
- 32 B. S. Pilgrim and N. R. Champness, *ChemPlusChem*, 2020, **85**, 1842–1856.
- 33 Q. Sun, L. Qin, C. Lai, S. Liu, W. Chen, F. Xu, D. Ma, Y. Li, S. Qian, Z. Chen, W. Chen and H. Ye, *J. Hazard. Mater.*, 2023, **447**, 130848.
- 34 S. Bandi, A. K. Pal, G. S. Hanan and D. K. Chand, *Chem.–Eur. J.*, 2014, **20**, 13122–13126.
- 35 M. D. Johnstone, E. K. Schwarze and G. H. Clever, *Chem.–Eur. J.*, 2015, **21**, 3948–3955.
- 36 K. Yazaki, M. Akita, S. Prusty, D. K. Chand, T. Kikuchi, H. Sato and M. Yoshizawa, *Nat. Commun.*, 2017, **8**, 15914.
- 37 D. Preston, J. E. M. Lewis and J. D. Crowley, *J. Am. Chem. Soc.*, 2017, **139**, 2379–2386.
- 38 G. Sarada, A. Kim, D. Kim and O.-S. Jung, *Dalton Trans.*, 2020, **49**, 6183–6190.
- 39 H. Dasary, M. Sarkar and D. K. Chand, *Chem. Commun.*, 2022, **58**, 8480–8483.
- 40 S. Samantray, S. Krishnaswamy and D. K. Chand, *Nat. Commun.*, 2020, **11**, 880.
- 41 S. S. Mishra, S. Krishnaswamy and D. K. Chand, *J. Am. Chem. Soc.*, 2024, **146**, 4473–4488.
- 42 X. Huang and Q. Zhang, *Acta Chim. Sin.*, 2023, **81**, 217–221.
- 43 D. K. Chand, K. Biradha, M. Kawano, S. Sakamoto, K. Yamaguchi and M. Fujita, *Chem.–Asian J.*, 2006, **1**, 82–90.
- 44 J. N. Kremsky, B. Szczepankiewicz, H. Toop and J. Morris, Nicotinamide riboside analogs, pharmaceutical compositions, and use thereof, *US Pat.*, 11180521B2, 2021.
- 45 S. P. Gaynor, M. J. Gunter, M. R. Johnston and R. N. Warrener, *Org. Biomol. Chem.*, 2006, **4**, 2253–2266.
- 46 S. M. Jansze, G. Cecot, M. D. Wise, K. O. Zhurov, T. K. Ronson, A. M. Castilla, A. Finelli, P. Pattison, E. Solari, R. Scopelliti, G. E. Zelinskii, A. V. Vologzhanina, Y. Z. Voloshin, J. R. Nitschke and K. Severin, *J. Am. Chem. Soc.*, 2016, **138**, 2046–2054.

